Ariadne-1: A Vital Drosophila Gene Is Required in Development and Defines a New Conserved Family of RING-Finger Proteins

Miguel Aguilera, Mariano Oliveros, Manuel Martínez-Padrón, Julio A. Barbas and Alberto Ferrús

Instituto Cajal, Consejo Superior de Investigaciones Científicas, Madrid 28002J, Spain

Manuscript received February 21, 2000
Accepted for publication March 27, 2000

ABSTRACT

We report the identification and functional characterization of *ariadne-1* (*ari-1*), a novel and vital Drosophila gene required for the correct differentiation of most cell types in the adult organism. Also, we identify a sequence-related gene, *ari-2*, and the corresponding mouse and human homologues of both genes. All these sequences define a new protein family by the *A*cid-rich, *R*ING finger, *B*-box, *R*ING finger, *c*oiled-*c*oil (ARBRCC) motif string. In Drosophila, *ari-1* is expressed throughout development in all tissues. The mutant phenotypes are most noticeable in cells that undergo a large and rapid membrane deposition, such as rewiring neurons during metamorphosis, large tubular muscles during adult myogenesis, and photoreceptors. Occasional survivors of null alleles exhibit reduced life span, motor impairments, and short and thin bristles. Single substitutions at key cysteines in each RING finger cause lethality with no survivors and a drastic reduction of rough endoplasmic reticulum that can be observed in the photoreceptors of mosaic eyes. In yeast two-hybrid assays, the protein ARI-1 interacts with a novel ubiquitin-conjugating enzyme, UbcD10, whose sequence is also reported here. The N-terminal RING-finger motif is necessary and sufficient to mediate this interaction. Mouse and fly homologues of both ARI proteins and the Ubc can substitute for each other in the yeast two-hybrid assay, indicating that ARI represents a conserved novel mechanism in development. In addition to ARI homologues, the RBR signature is also found in the Parkinson-disease-related protein Parkin adjacent to an ubiquitin-like domain, suggesting that the study of this mechanism could be relevant for human pathology.

THE genes encoded in the 16F region of the X chromosome of Drosophila are the subject of thorough structural and functional analysis because of their involvement in neural development (Ferrús *et al.* 1990; Prado *et al.* 1999). We report here the characterization of the gene *ariadne-1* (*ari-1*) and its encoded RING-finger protein ARI-1. The RING-finger motif is a cysteine-rich structure first identified in the human *R*eally *I*nteresting *N*ew *G*ene 1 (*RING-1*; Lovering *et al.* 1993). Its structure has been solved by ^{1}H-NMR methods for the immediate early IE110 equine herpes virus protein (Barlow *et al.* 1994) and the promyelocytic leukemia proto-oncoprotein PML (Borden *et al.* 1995). In both cases, the motif coordinates two zinc ions (Klug and Schwabe 1995) in the characteristic "cross-brace" system. RING-finger motifs have now been reported in a large number of proteins in many species (Borden and Freemont 1996), and they are involved in various functions including growth control, signal transduction, viral pathogenicity, and peroxisome biogenesis (Saurin *et al.* 1996). Although the motif has been shown to be essential for some of these functions, the precise interactions in which it is involved is, in most cases, unknown. It is generally assumed that this motif directly mediates protein-protein interactions although specific examples are still scarce. The herpes simplex virus protein Vmw110 requires its RING finger to localize to the kinetochore and promote CENP-C degradation through the ubiquitin pathway (Everett *et al.* 1999). Also, the N-terminal RING motif of human SIAH-1 mediates the targeting of DCC (*D*eleted in *C*olorectal *C*ancer) for ubiquitin-mediated proteolysis (Hu and Fearon 1999). The recent biochemical characterization of Skp1-Cdc53/CUL1-F-box (SCF) and anaphase promoting complex (APC) ubiquitination complexes suggests that RING fingers play a central role in the combinatorial set of protein interactions that determine substrate specificity in the ubiquitin pathway (Tyers and Willems 1999).

This pathway targets proteins for degradation through the 26S proteasome (Hershko and Ciechanover 1998). It is considered a mechanism that can quantitatively regulate substrates such as cyclins, transcription factors, hormone nuclear receptors, and oncoproteins. Four types of enzymes are known to mediate ubiquitination: ubiquitin-activating (referred to as E1 or Uba), ubiquitin-conjugating (E2 or Ubc), ubiquitin-substrate ligase (E3 or Ubr), and the recently discovered polyubiquitinating ligase (E4; Koegl *et al.* 1999). E2 enzymes constitute a family of variants in all species analyzed. Thus, 9 Ubc genes are known in Drosophila, 13 in yeast, 4 in mice, and 8 in humans (Matuschewski *et al.* 1996). Mutations in Drosophila and mice Ubc genes lead to

Corresponding author: A. Ferrús, Instituto Cajal (CSIC), Ave. Dr. Arce 37, Madrid 28002, Spain. E-mail: aferrus@cajal.csic.es

lethality (Harbers *et al.* 1996; Cenci *et al.* 1997), demonstrating that the different family members are not functionally equivalent. However, the biological significance of this multiplicity of enzymes remains unclear. Recent evidence has uncovered an additional role for some E1 and E2 enzymes, namely, the tagging of proteins with SUMO-1 or Rub-1 instead of ubiquitin (Desterro *et al.* 1997; Liakopoulos *et al.* 1998). This alternative pathway, albeit related to ubiquitination, leads to the modulation of protein activity rather than proteolysis (Hodges *et al.* 1998). On the other hand, the existence of stable ubiquitinated proteins (*e.g.*, histones) and enzymes that reverse ubiquitination suggest that this process might be more elaborately controlled than previously thought.

The role of ubiquitin and ubiquitin-like systems has been documented in several aspects of cell regulation, including the cyclin-dependent progression through the mitotic cycle (Hershko 1997) and NF-κB-dependent gene expression (Baldwin 1996). However, neural development is emerging as a novel scenario, as suggested by the defects in the ubiquitin pathway elicited in Drosophila *bendless* mutants (Muralidhar and Thomas 1993; Oh *et al.* 1994). In humans, mutations in the *parkin* gene, whose corresponding protein contains an ubiquitin-like domain, cause juvenile parkinsonism through selective neuronal depletion (Kitada *et al.* 1998). We report a novel Drosophila RING-finger protein, ARI-1, which is required for neural development. Null mutations in this gene yield occasional adult survivors with short life span, motor behavioral deficits, and abnormal connectivity in the central nervous system. The protein interacts with a novel Ubc enzyme specifically through one of the RING-finger motifs and is structurally related to Parkin. In addition, we identify in Drosophila a closely related gene, *ariadne-2*, which in conjunction with the corresponding murine and human homologues, defines a new conserved protein family.

MATERIALS AND METHODS

Nomenclature, fly strains, and genetic procedures: The name *ariadne* refers to the apparent loss of clues to find the correct path of axonal projection, and it evokes the Greek myth of the thread that Ariadne gave to Theseus to find his way in the Minotaur's labyrinth. The four *ari-1*$^{1-4}$ alleles had been referred to previously as *l(1)1199*, *l(1)3747*, *l(1)4822*, and *l(1)5777* (Ferrús *et al.* 1990), respectively. The insertional duplication *Dp(1;3)JC153* (*Dp* for brevity) is routinely used to cover the lethality of *ari* alleles and the flanking markers *wupA* and *os*. The rearrangement *Dp(1;3)JC153*$^{R4\text{-}III}$ and *Dp(1;3)JC153*^{R5} are X-ray derivatives from *Dp* (Prado *et al.* 1999). The four *ari* alleles were induced on *y w wupA*^{hdp3} (*ari-1*^{2}, *ari-1*^{3}, and *ari-1*^{4}) or *f*^{5} *os* (*ari-1*^{1}) marked chromosomes. The *f*^{5} marker was exchanged for *y w* by recombination. Gynandromorph mosaics were obtained using the unstable *R(1)2, In(1)w*^{vC} chromosome. Somatic mosaics were obtained among the X-ray-treated adults of genotype *y w ari-1*/M(1)n* (24–48 hr after egg laying). Germline mosaics were induced by X-ray treatment of *ovo*^{D1} *v/y w ari-1** larvae. The viability and oogenesis of transheterozygous mutant combinations were analyzed in the offspring from the cross: *y w ari-1*/FM6* × *y w ari-1** ; *Ki Sb Dp/TM3*. The lethal phase was estimated following the development of eggs from the cross: *y w ari-1*/+* × CS. Groups of 20–30 eggs were plated on petri dishes with humid filter paper and drops of yeast, counting the living individuals every 24 hr.

Nucleic acids procedures: Drosophila embryo, adult, and head cDNA libraries (provided by B. A. Hamilton, S. Orgad, and C. Salvaterra) were screened with genomic probes from phages E511 and M509 (Baumann *et al.* 1987). A total of nine overlapping cDNA fragments (1.2–2.5 kb) were subcloned and sequenced using standard techniques (Sambrook *et al.* 1989). Northern blots were performed on 5 μg of purified mRNA (Micro mRNA purification kit, Pharmacia, Piscataway, NJ) and hybridized with two probes, a cDNA fragment encompassing the *ari-1* coding region and a *D-ras* cDNA as an internal control for densitometric quantitation (Molecular Dynamics, Sunnyvale, CA). Coding sequences from *ari-1* mutants were analyzed after duplicate mRNA isolation from male third-instar larvae (Micro mRNA purification kit, Pharmacia), reverse transcription (First-Strand cDNA synthesis kits, Pharmacia), and PCR amplification with Pfu proofreading thermostable DNA polymerase (Stratagene, La Jolla, CA) using suitable flanking oligonucleotides (5′-dGAGGATCCAAGCAGTAACGCA AAACAG-3′; 5′-dGCGAATTCGGCTTAGCTTAGTTATCAG-3′). Human cortex, caudate, pancreas, liver, and kidney cDNA libraries (provided by J. R. Naranjo) were screened by PCR amplification with specific nested primers (sequence available upon request) and cloning-site flanking oligonucleotides in λgt10, λgt11, λDR2 vectors. The same procedure was followed to screen mouse embryo and brain cDNA libraries (provided by J. R. Naranjo, A. Nieto, and M. Torres).

Immunological procedures: Monospecific anti-ARI-1 serum used for Figures 3 and 4 was obtained from rabbit antisera raised against an ARI-1 C-terminal synthetic peptide, CGYD KEWWEYTE, covalently coupled to KLH (Sigma, St. Louis). A GST-ARI-1 chimeric protein was made by subcloning of a cDNA fragment coding for amino acids 129–503 in the pGEX-3X vector (Pharmacia). Protein extracts from *Escherichia coli* expressing this fusion were subjected to SDS-PAGE, transferred to nitrocellulose filters, and used for affinity purification of monospecific antibodies from the crude sera. This protocol was also followed with other rabbit and mouse sera generated against various fragments of ARI-1 expressed in *E. coli* or fusions with glutathione-S-transferase (GST), maltose-binding protein, or 6-His tag. Protein extracts for Western blots were normalized for total protein content. In the cellular fractionation Western blots, nuclear extracts from brown or black pupae were obtained as reported (Preston *et al.* 1988).

Histological procedures: Holmes-Blest silver staining was done on paraffin-embedded 10-μm sections (Blest 1975). The embryo central nervous system (CNS) structure was visualized with the neural-specific monoclonal antibody 22C10 (Fujita *et al.* 1982) followed by a fluoresceine-labeled secondary antibody. Toluidine blue and β-galactosidase staining were performed as described (Ashburner 1989). Electron microscopy procedures were as previously described (Canal *et al.* 1994). For *in situ* hybridization, digoxigenin-labeled sense and antisense RNA probes were synthesized from linearized plasmids containing the complete coding region of *ari-1* in pBluescript-KS+ vector (Stratagene) using T3 and T7-RNA polymerases (Pharmacia) and a DIG RNA labeling mix (Boehringer Mannheim, Indianapolis) according to the manufacturers' instructions. Paraffin sections were hybridized following standard procedures (Ashburner 1989).

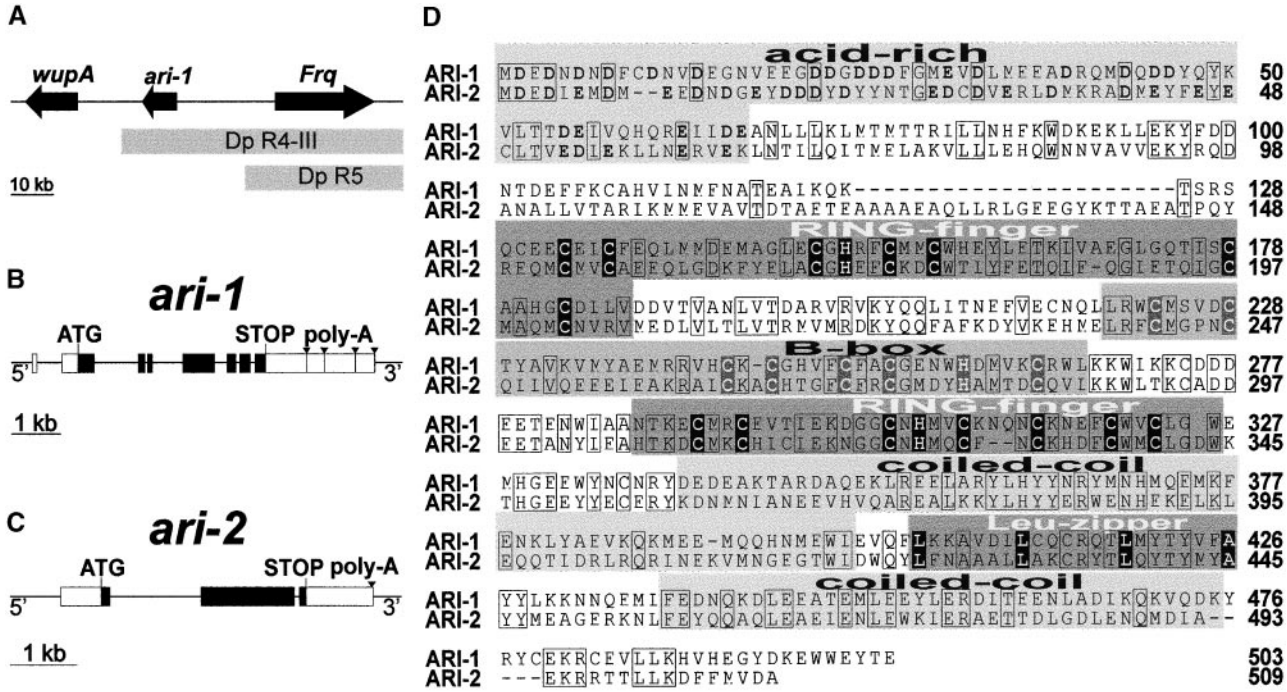

Figure 1.—The *ari* genes. (A) The gene *ari-1* is located in the 16F region on chromosome X between the breakpoints of *Dp(1;3)JC153*$^{R4\text{-}III}$ (*DpR4-III* for brevity) and *Dp(1;3)JC153*^{R5} (*DpR5*). The flanking Frequenin (*Frq*) and troponin I (*wupA*) encoding genes are indicated. The centromere is to the right. (B) *ari-1* exon/intron structure (open boxes) and coding region (solid boxes). Four polyadenylation signals (▼) are indicated in the 3′ UTR. (C) *ari-2* exon/intron structure. (D) Sequence alignment of ARI-1 and ARI-2 proteins. Identical amino acids are boxed and structural motifs are shaded. Acid residues of acid-rich regions are shown in boldface. Consensus C/H residues are shaded black or dark gray, and key L residues are shaded in black.

Functional tests: Electroretinograms (ERG) were recorded from immobilized adult flies as described (Canal *et al.* 1994). Wing beat frequency was measured in single flies according to Prado *et al.* (1995). Flight performance also was evaluated as in Drummond *et al.* (1991). The flip-over test was done as follows. Since *ari-1* adult survivors of null alleles are flightless, single individuals were placed on a small petri dish for observation. A single-hair brush was used to flip flies upside down and the time to recover upright position was measured. Other flightless (*e.g.*, *Cy* mutant) *ari*$^{+}$ flies take consistently <1 sec to stand up. The same observation chambers were used for courtship activity of single pairs of mutant males and wild-type females.

Two-hybrid interaction assays: To analyze protein-protein interactions, the MATCHMAKER Two-Hybrid System 2 kit (Clontech, Palo Alto, CA) was used. Wild-type and mutant *ari-1* complete coding sequence (CDS), and restriction fragments were obtained from sequenced plasmids described above. *ari-2* and *ubcD10* CDS were PCR amplified from larval Canton-S (CS) cDNA samples using proofreading thermostable Pfu DNA polymerase (Stratagene) and suitable primers (*ari-2*: 5′-dCCGAATTCGCCAATCCGCCGGAATGGACTC-3′/5′-dCGTCGTTGGGCCTACTACTAGATGGATAC-3′; *ubcD10*: 5′-CCGGATCCACATAGACATCACGATGACTGCG 3′/5′-dCCCACCTCCTCGAGCTCTACCTCCGCCTATCC-3′). All fragments were subcloned in pACT-2 and/or pAS2-1 vectors, encoding GAL4 activation and DNA-binding domains, respectively. Linker regions were always sequenced to discard frameshifts or errors due to subcloning procedures. *ari-2* and *ubcD10* constructs were fully sequenced to detect artifactual mutations due to PCR amplification. *Saccharomyces cerevisiae* Y190 strain was used for all transformations, and β-galactosidase filter assays were carried out during 2 hr or less according to the manufacturer's instructions.

RESULTS

The *ariadne-1* (*ari-1*) gene is defined by four allelic ethyl methanesulfonate-induced lethal mutants, *ari-1*^{1}, *ari-1*^{2}, *ari-1*^{3}, and *ari-1*^{4}, mapping between the *DpR4-III* and *DpR5* breakpoints in the 16F region of the X chromosome (Prado *et al.* 1999). This chromosomal segment was cloned, sequenced to a large extent, and the genes harbored therein analyzed in detail. The *ari-1* transcription unit is located between the Frequenin and Troponin I encoding genes, *Frq* and *wupA*, respectively (Figure 1A).

Ariadne-1 leads a new conserved family of proteins with the ARBRCC signature: The *ari-1* transcription unit extends over 8 kb of genomic DNA (see appendix for all GenBank nucleotide and SPTREMBL protein database accession numbers). After screening adult and embryo libraries, nine overlapping cDNAs were isolated that account for the longest mRNA (4.3 kb) out of the four bands detected in Northern blots (Figure 3A). There was no evidence of alternative splicing among the cDNA sequences. Instead, the long 3′ untranslated region (UTR) contains four polyadenylation signals (Figure 1B), and hybridization of Northern blots with suitable

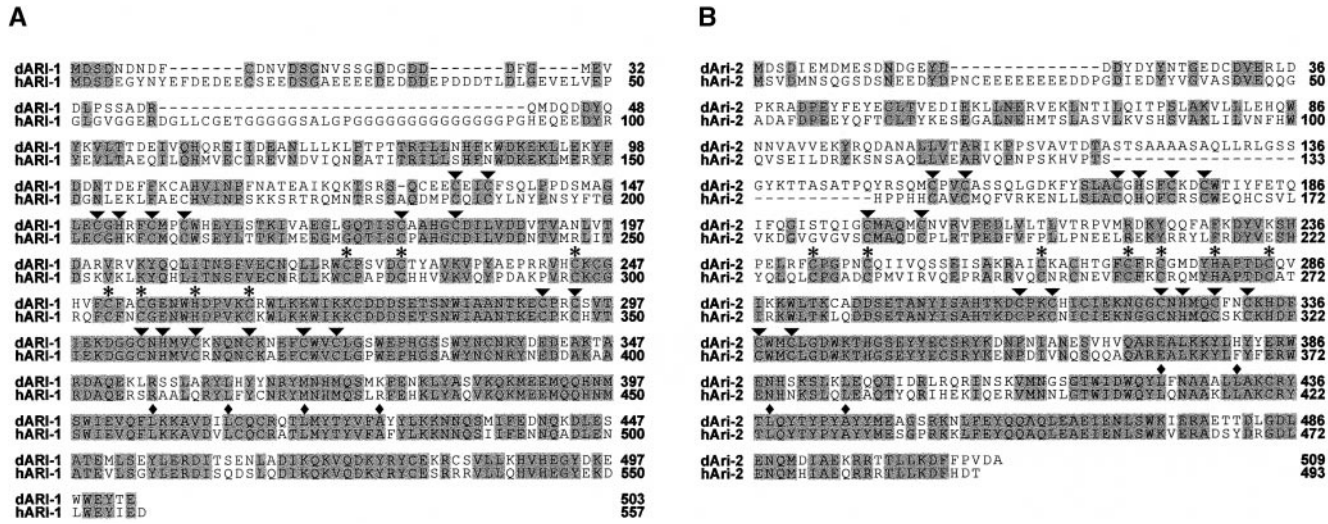

Figure 2.—ARI human homologs. (A) Sequence alignment of Drosophila ARI-1 (dARI-1) and human (hARI-1) proteins. (B) Equivalent alignment with ARI-2. Identical amino acids are shaded. Consensus C/H residues are indicated in the two RING fingers (▼) and the B-box (*) motifs, and key residues of the leucine-zipper are also labeled (◆).

cDNA fragment probes demonstrated that each mRNA corresponds to the lengths deduced from the four polyadenylation sites (not shown). The coding sequence predicts a 503-amino-acid protein of 59 kD without any significant homology to functionally characterized proteins (Figure 1D). *S. cerevisiae* and *Caenorhabditis elegans* data from genome sequencing projects report putative homologues with 35 and 56% identity, respectively (see appendix). In addition, expressed sequence tags (EST) database searches revealed fragments of putative ARI-1 homologues in mouse and humans. We screened human and mouse cDNA libraries by PCR using specific nested primers. The predicted coding sequence from the isolated clones, although incomplete, indicates a protein 68% identical to Drosophila ARI-1 within the 463 amino acids sequenced. Recently, the complete human ARI-1 sequence has been reported in the database (see appendix; Figure 2A). Mouse and human ARI-1 sequences are 98% identical.

Sequence comparison of ARI-1 with Drosophila databases revealed a region of significant homology in the genomic P1 clone DS02833 that maps to bands 58C2–7. Three cDNA clones from the Berkeley *Drosophila* Genome Project (BDGP) with 5′ ESTs upstream to the homologous region were found to encode a protein 32% identical to ARI-1, which we named ARI-2 (Figure 1, C and D). As in ARI-1, database searches and EST contigs served to identify ARI-2 homologues in *C. elegans*, *Mus musculus*, and *Homo sapiens*. The complete coding sequence was derived for the three representatives, although there is no functional information about any of them. Mouse and human sequences are 97% identical to each other and, in turn, 51% identical to Drosophila ARI-2 (Figure 2B).

Comparison of ARI-1 and ARI-2 with their counterparts in other species provides evidence for a modular structure with three main regions described from the amino terminus: an acid-rich domain, a cysteine- and histidine-rich (C/H) domain, and a putative coiled-coil forming domain (Figure 1D). The acidic region is the least conserved in terms of its primary sequence but it is present in all family members as a cluster of aspartic and glutamic residues. The most conserved stretch is the cysteine/histidine-rich region, which exhibits three putative Zn^{2+} coordinating motifs: two RING fingers (Freemont 1993) and one B-box (Reddy and Etkin 1991). All Zn^{2+} coordinating positions, as well as the accepted variations in C/H substitutions or changes in spacer length with respect to the original consensi (Carthew and Rubin 1990), are found in ARI-1, ARI-2, and their corresponding homologues (Price *et al.* 1993; Régnier *et al.* 1995; Tranque *et al.* 1996). Finally, the highly conserved C-terminal third of both ARI proteins shows two segments containing heptad repeats of hydrophobic residues with a high probability (up to 92% score in the 341–400 amino acid interval) to form a coiled-coil structure (Lupas *et al.* 1991). Between the two putative coiled-coils is a leucine-zipper motif suitable to form an α-helical structure (Figure 1D) (Landschulz *et al.* 1988).

A string of RING-finger/B-box/RING-finger/coiled-coil motifs, akin and with similar spacing, is also found in proteins of the RBCC family, particularly those having two B-boxes (R/B1/B2/CC; Reddy *et al.* 1992). In this context, the ARI family presents the novelty of having a second RING finger instead of B2. We screened the available databases for RBR-containing sequences and a number of variants were found in which the RBR signature appears in combination with other motifs (appendix). One notorious RBR-containing protein is Par-

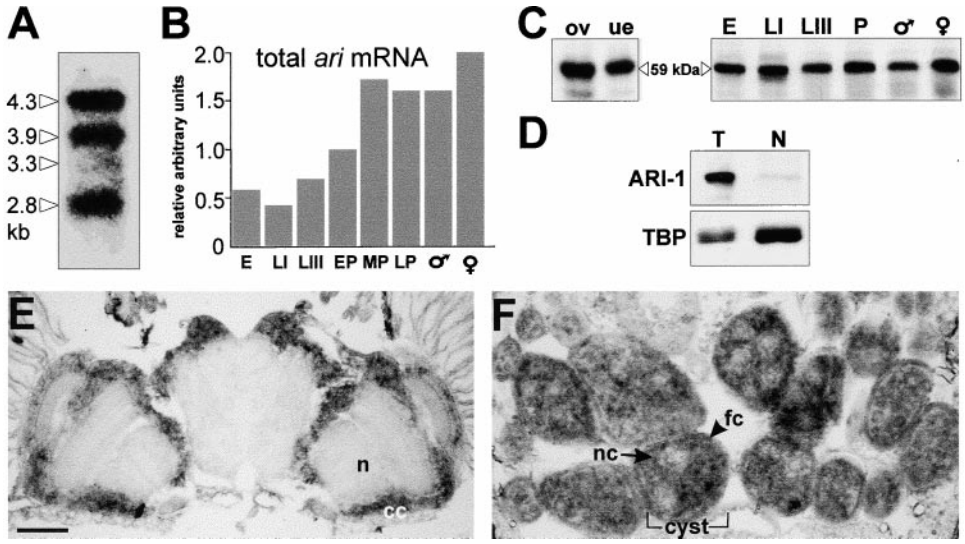

Figure 3.—*ari-1* expression. (A) Northern blot from CS wild-type larvae probed with *ari-1* cDNA. (B) Densitometric quantitation of total *ari-1* mRNA in arbitrary units during development using Drosophila *ras* mRNA as an internal control. E, 0- to 18-hr embryos; LI, LIII, first- and third-instar larvae; EP, MP, LP, white, brown, and black pupae, respectively; ♂, ♀, adult males and females. (C) Developmental Western blot probed with an affinity-purified antibody against ARI-1 protein. ov, ovarioles; ue, unfertilized eggs; E, 6- to 8-hr embryos; LI, first-instar larvae; LIII, third-instar larvae; ♂, ♀, adult males and females. Note the signal in unfertilized eggs that demonstrates the maternal deposition of ARI-1. All lanes contain the same amount of total protein, on the basis of Coomassie blue staining and densitometry. (D) Western blot of nuclear (N) or total (T) fractions obtained from 0- to 18-hr embryos. As a control, the same blot was probed with an anti-TBP (TATA binding protein) antibody. (E) *In situ* hybridization of a digoxigenin-labeled probe to a paraffin-embedded horizontal section of normal adult brain and optic ganglia. The signal is distributed throughout all neural centers. n, neuropile; cc, cellular cortex. (F) The same hybridization showing adult ovarioles. Nurse (nc) and follicular (fc) cells in every cyst show *ari-1* transcription. Anterior is toward the top. Bar, 60 μm (E and F).

kin, a causal element of Parkinson's disease (Kitada *et al.* 1998) that presents the RBR string located C-terminal to an ubiquitin-like domain. Furthermore, the unusual four-instead-of-two spacing between Cys4 and Cys5 in the R2 motif of ARI-1 is also present in this human protein.

***ari-1* is expressed in most tissues and developmental stages:** The four mRNA isoforms encoding ARI-1 are expressed at all developmental stages at increasing levels from embryogenesis onward (Figure 3B). Maximum levels are reached during metamorphosis and maintained in the adult. *ari-1* mRNA is detected in all tissues, with prominent levels in the adult nervous system (Figure 3E) and female gonads. In the ovaries, *ari-1* expression is detected in follicular as well as nurse cells in each cyst (Figure 3F). The expression is also ubiquitous in larval stages (not shown). Western blots using several affinity-purified antisera detected a single 59-kD protein band in agreement with the theoretical M_r (Figure 3C). The specificity of this signal is proven by the fact that it is not observed in protein extracts from null mutants (see below) and it is recovered by the chromosomal fragment *DpR4-III* that contains a normal copy of the gene. Protein expression is detected in the maternal deposit of unfertilized egg extracts (Figure 3C) and at all succeeding developmental stages. All monospecific, affinity-purified sera generated so far ($n = 12$) against ARI-1 fusion proteins or peptides have been ineffective in immunohistology. Thus, the subcellular localization was studied by Western blot using nuclear and cytoplasmic fractions. The ARI-1 band was detected in the total but not the nuclear enriched fractions (Figure 3D), suggesting that ARI-1 localizes mainly in the cytoplasm (however, see discussion).

Structural bases of *ari-1* alleles: The *ari-1* coding region was sequenced in the four available alleles. *ari-1*^{1} and *ari-1*^{4} show single base substitutions generating STOP codons after amino acids 128 and 91, respectively (Figure 4C). Both proteins would lack the RBRCC domains and are not detected in Western blots. On the basis of these alterations, we consider *ari-1*^{1} and *ari-1*^{4} alleles as null mutations. Alleles *ari-1*^{2} and *ari-1*^{3} are also point mutations, but lead to single amino acid substitutions at key cysteine residues of each R motif, C150Y in *ari-1*^{2} and C309Y in *ari-1*^{3} (Figure 4C). These mutations are likely to prevent Zn^{2+} coordination, thus modifying the tertiary structure and function of ARI-1, a phenomenon demonstrated for BRCA-1 (Brzovic *et al.* 1998). Western blots of larval extracts indicate that while the normal 59-kD band is absent in *ari-1*^{1} and *ari-1*^{4}, it remains in *ari-1*^{2} and *ari-1*^{3} (Figure 4B).

Null *ari-1* mutant survivors show motor task defects: The four mutant alleles show the same lethal phase at the pupal stage (Figure 4A). However, null alleles *ari-1*^{1} and *ari-1*^{4} allow adult male survivors at low frequency (<10%) while *ari-1*^{2} and *ari-1*^{3} have never been recovered as adults in any type of cross. The escapers recovered were tested for several motor behaviors including flight, courtship, grooming, and time required to recover the upright position after flipping over (see materials and methods). The null escapers performed poorly in all of these motor tasks. All individuals neither jump nor fly, exhibiting a wing beat frequency (190 Hz ± 17, $n = 24$) well below normal (230 Hz ± 10 in

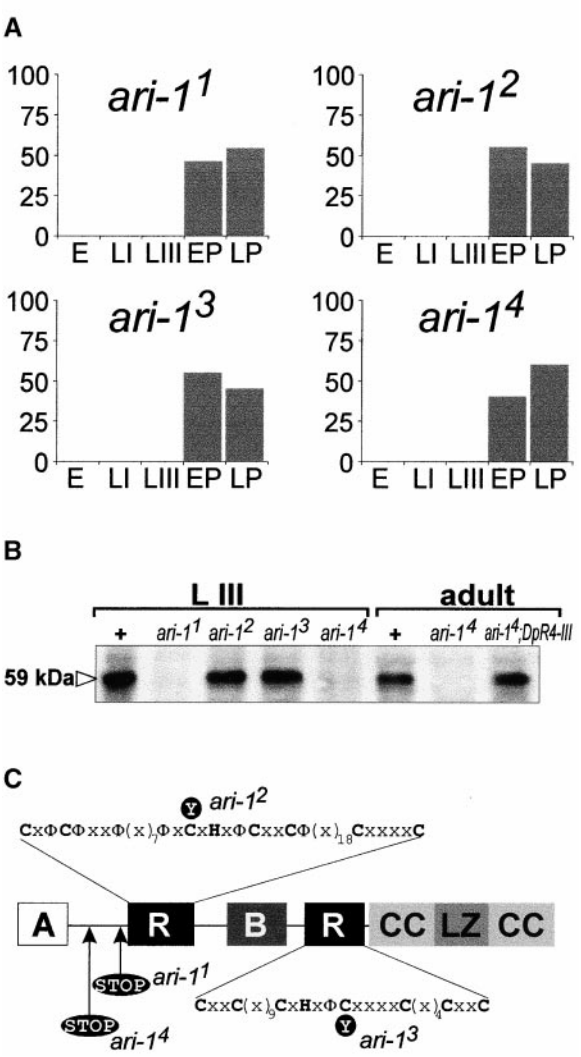

Figure 4.—*ari-1* mutations. (A) Mutant lethal phases. The following number of eggs (n) and percentage of dead (d) individuals were counted: *ari-1*^{1} (n = 297, d = 28%), *ari-1*^{2} (n = 315, d = 29%), *ari-1*^{3} (n = 320, d = 25%), and *ari-1*^{4} (n = 250, d = 24%). (B) Western blot of normal (+) and mutant larvae and adults labeled with anti-ARI-1 affinity-purified serum. The null condition in *ari-1*^{4} adult escapers is rescued by *DpR4-III*, demonstrating that the antibody recognizes the structural product of this gene. (C) Mutations in *ari-1*^{1} and *ari-1*^{4} lead to STOP codons near the N terminus, while *ari-1*^{2} and *ari-1*^{3} are single amino acid substitutions in residues involved in Zn^{2+} coordination.

sibling controls). These data were obtained from 1- to 3-day-old adults. Also, they failed to perform any of the sexual routines (wing song, dance, licking, and mounting) in front of wild-type females (n = 32). Grooming activity was apparently normal when exhibited. The time required to recover upright position varied greatly among individuals but in general, the values deteriorated with age. Day-old flies usually recovered in <1 sec while flies older than 7 days took 30 sec or more to stand up. Life span ranged from 2 to 28 days (n = 41), with flies displaying continuous tremors and frequently falling during the final 24 hr. By contrast, most sibling controls lived over 50 days.

Consistent with the ubiquitous expression of the gene, morphological phenotypes were identified in most tissues analyzed in the survivors. Bristles appeared shorter and thinner than normal although their number and pattern were not modified. Among the thoracic muscles, the tergal depressor of the trochanter (TDT) shows the most severe defects in the fiber assembly (Figure 5H). Other muscles appear structurally normal at this level of observation although their size is reduced to a variable extent. In all probability, these muscle phenotypes may be the cause of the effects on jumping and reduced wing beat frequency. All morphological phenotypes, including the neural traits (see below), are identified in gynandromorphs and somatic mosaics. The latter type of mosaics allow us to conclude that *ari-1* is a cell autonomous function. Since the nervous system and ovaries exhibit the higher levels of expression, we analyzed in greater detail the phenotypes in these organs.

Neural connectivity defects are a major trait of *ari-1* phenotypes: The mutant larval nervous system was examined through several staining procedures including monoclonal antibody 22C10 to visualize neurons, anti-chaoptin to visualize the pattern of projecting photoreceptors, toluidine blue to visualize the general CNS organization and viability of cells, and X-gal in 10 *tau-lacZ* enhancer trap lines with selective expression patterns. No overt or consistent morphological defects were detected by these procedures (not shown). By contrast, adult escapers of null alleles as well as gynandromorph mosaics showed major projection defects in the brain and thoracic ganglia (Figure 5, A–F). Misrouted axonal tracts were detected in all preparations visualized by silver staining, although the extent of the abnormality varies within and between individuals. Very often, the medulla of the optic ganglion appeared rotated with respect to the lamina or exhibited grossly abnormal projections. For example, the optic tract between the medulla and the lobula complex may project directly toward the brain instead (Figure 5B). Also, the chiasm between the lamina and the medulla may appear split, sending a subset of fibers directly to the lobulla. In the brain and thoracic ganglia, new or aberrant versions of normal axonal bundles are found (Figure 5, C and D). Occasionally, a major bundle is missing, such as the descending path that carries one of the two cervical giant fibers (Figure 5F). It is important to note that the aberrant projections do not seem to result from fasciculation defects or growth impairments. All abnormal bundles consist of coherent groups of axons that project along unusual paths rather than disorganized or aborted individual axons. Thus, the connectivity phenotypes appear to result from wrong decisions or signals affecting the leading growth cone rather than general-

ized adhesion defects. The size of the brain and the general organization of neural centers are essentially normal, with no histological signs of cell death by necrosis. These observations suggest that *ari-1* activity is not required for cell division or survival. This conclusion is further supported by the normal size of adult somatic mutant tissue observed in gynandromorphs. Since neither the embryo nor the larval CNS have detectable structural defects, the observed adult phenotypes must be generated mainly at the pupal stage. This is in agreement with the high levels of ARI-1 protein found in normal pupae (Figure 3B). Also, the lethal phase of the four alleles corresponds to this stage (Figure 4A), suggesting that ARI-1 is in particularly high demand at this developmental stage. Since this is the time of metamorphosis, when a thorough reorganization of neural connections takes place, the adult neural phenotypes appear justified. It could be argued, however, that the lack of embryonic or larval phenotypes could be due to a long-lasting perdurance of maternal deposits during oogenesis. This alternative seems unlikely because null mutant individuals obtained from germline mosaics (see below) do not show more severe phenotypes than those of regular adult escapers from heterozygous mothers.

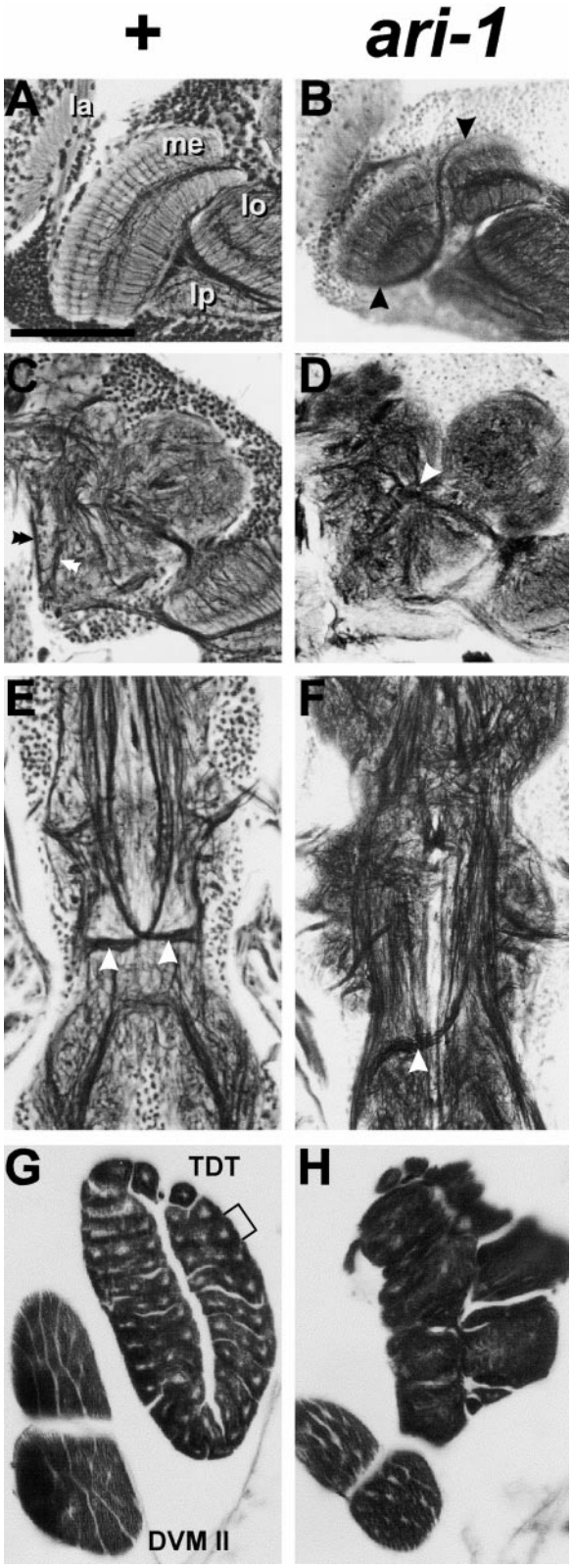

Structural and functional *ari-1* mutant phenotypes in photoreceptors: To analyze the mutant phenotype at the subcellular level, we relied on the adult photoreceptors because their ultrastructure and functional properties are well characterized in the normal type. In adult mosaic retina ($n = 6$), *ari-1*^{2} photoreceptors exhibit a 13% reduction in the average R1-6 rhabdomere area (normal = 2.20 ± 0.03, mutant = 1.90 ± 0.04 μm^2, n = 36). Ultrastructural analysis of these eyes revealed a severe reduction of the rough endoplasmic reticulum

Figure 5.—*ari-1* phenotypes. Silver-stained sections of adult mutant mosaics or escapers showing structural defects in the nervous system and selected muscles. (A) Normal CS optic ganglion. la, lamina; me, medulla; lo, lobula; lp, lobula plate. (B) Equivalent view from an *ari-1*^{2} gynandromorph showing the mutant side. Note the aberrant bundle of axons (arrows) crossing the medulla. This projection should have been directed to the lobula complex. (C) Right side view of the central brain in CS. Two normal bundles running parallel to the esophageal opening are indicated by double arrowheads. (D) Equivalent section from an *ari-1*^{4} adult escaper. Note that the two normal bundles indicated in C are absent in the mutant. Also, an abnormal fusion of several axonal tracts is marked by an arrow. (E) Thoracic ganglion of a normal adult. The two major descending tracts containing the cervical giant fiber and their characteristic contralateral crossing at the border between the meso- and metathoracic neuromeres are indicated (arrows). (F) Equivalent view from an *ari-1*^{4} adult escaper. Note the absence of the left descending tract. Arrow indicates the normal right tract that remains. (G) Normal tubular TDT and fibrillar DVMII muscles from the thorax of a CS wild-type adult. One of the fibers that compose the TDT is marked with a bracket. (H) The same muscles in *ari-1*^{1}/*ari-1*^{2} females. Note the severe structural defects in the TDT while the DVMII appears reduced in size but with relatively normal structure at this level of observation. Bar, 60 μm (A and B), 45 μm (C and D), 130 μm (E and F), and 115 μm (G and H). Anterior is toward the top.

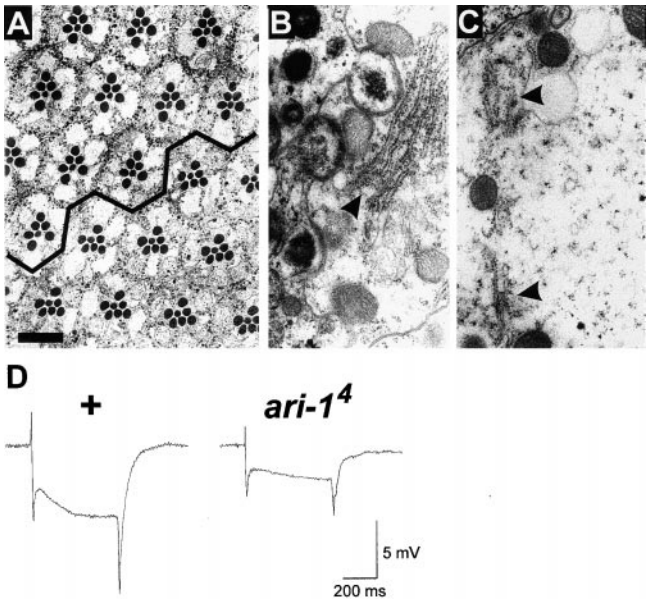

Figure 6.—Structural and functional phenotypes in photoreceptors. (A) Limit of a mosaic *ari-1*^{2} retina identified by the *white* marker. Ommatidia above the black line are normal and show the regular pigment granules. (B) Normal photoreceptor showing the RER (arrowhead). (C) Representative case of a mutant photoreceptor. Note the scarce RER (arrowhead) and the abundant particles of ribosome-like size. (D) Electroretinograms from normal and mutant eyes. Traces represent the average of 20 recordings. Note the substantial reduction of the sustained negative components as well as the amplitude of the ON and OFF transients. Bar, 10 μm (A) and 300 nm (B and C).

(RER) in the mutant versus adjacent normal cells (Figure 6C). This reduction was observed in all photoreceptor types (R1-7, $n = 56$) within the mutant clone and it appeared consistently through sampling sections that span 0.91 μm deep into the retina. The functional performance of mutant eyes was assayed by ERG obtained from adult *ari-1*^{1} and *ari-1*^{4} escapers (Figure 6D). The negative sustained component was reduced to 1/3 (2.2 ± 0.4 mV, $n = 4$) of that from sibling controls (6.7 ± 0.5 mV, $n = 5$) or the contralateral eye in gynandromorphs ($n = 5$). This ERG component reflects phototransduction at the rhabdomeres. In addition, the amplitude of the ON and OFF transients appear reduced by ~30% (mutant = 3.0 ± 0.4 mV, normal = 4.3 ± 0.4 mV) and 60% (mutant = 3.0 ± 0.1 mV, normal = 7.7 ± 0.7 mV), respectively. These ERG components are thought to indicate the synaptic activity between the retina and the lamina (Coombe and Heisenberg 1986). Thus, the reduced phototransduction activity results, most likely, from the reduced rhabdomere surface while the reduced ON and OFF amplitudes could possibly result from connectivity defects and/or secretory impairments at synaptic terminals. In turn, the depleted RER could be the common origin of these structural and functional defects (see discussion). No signs of photoreceptor degeneration were evident among aged escapers.

TABLE 1

Germline mosaics

Allele	*N* females	Clones	F_1 offspring
ari-1^{1}	105	8	153
ari-1^{2}	108	3	0
ari-1^{3}	115	5	394
ari-1^{4}	288	9	371

Clones were induced in X-ray-treated *ovo*^{D1} *ari-1* larvae. N* is the total number of adult females screened. F_1 offspring is the total number of F_1 females obtained from the pool of clones. Four additional clones were obtained resulting from crossovers distal to the *ari-1* locus as deduced by the visible markers and the recovery of adult male progeny.

***ari-1* phenotypes in oogenesis: the differential effect of mutations in R1 and R2 motifs:** The study of mutant effects on ovaries was carried out in transheterozygous (*ari-1*^{x}/*ari-1*^{y}) females and germline mosaics. Transheterozygotes were attempted in all pairwise combinations of alleles but only the *ari-1*^{1}/*ari-1*^{2} genotype reached adulthood. Interestingly, the viability of this genotype is dependent on the direction of the cross. The paternal introduction of *ari-1*^{2} yields heterozygous F_1 daughters with 30% viability, while the yield for the same genotype drops to 3% if introduced maternally. This observation strongly suggests that a mutated version of ARI-1 in the first RING finger (R1) has a deleterious effect in oogenesis. Since this type of effect is usually sensitive to dosage, we manipulated the ratio of normal to mutated genes. As a source of an additional copy of the normal gene, we used the chromosomal fragment *Dp(1;3)JC153*. Mothers *ari-1*^{2}/+/+ yield *ari-1*^{1}/*ari-1*^{2} female offspring with 8% viability while *ari-1*^{2}/*ari-1*^{2}/+ females are sterile. The gene dosage and maternal effects on the viability of this genotype indicate a peculiar effect of the protein when mutated in the R1 motif. The ovarian structure of *ari-1*^{1}/*ari-1*^{2} and *ari-1*^{2}/*ari-1*^{2}/+ females shows a very mild effect consisting of an abnormally small number of ovarioles and occasional arrested cyst development.

Germline mosaics of the four alleles were induced in *ovo*^{D1}/*ari-1* by X rays at the larval stage. In this type of clone, the nurse cells and the oocyte are homozygous for the mutation while the adjacent follicular cells remain heterozygous. Clones were obtained with the four alleles tested (Table 1). The null alleles *ari-1*^{1} and *ari-1*^{4} do not prevent oogenesis, indicating that the normal function of ARI-1 is not essential for this process, even though the gene is transcribed in the ovaries (Figure 3F). Also, the observation that *ari-1*^{3}/*ari-1*^{3} clones maintain normal oogenesis indicates that the R2 motif, if mutated in a key cysteine, is not particularly deleterious in this process, at least in the nurse cells. However, clones homozygous for *ari-1*^{2} yield defective eggs unable to sustain development

irrespective of their zygotic genotype. These abortive embryos do not reach the blastoderm stage. In contrast, embryos from *ari-1*^{2}/*ari-1*^{2}/+ females (see above) reach more advanced stages, including the patchy differentiation of abdominal setae belts. Thus, a 2:1 ratio of mutant-to-normal gene copies shows a weaker effect than a 1:0 ratio. In this context, it should be noted that the 1:1 ratio of heterozygous females allows normal oogenesis and early development of all zygotic genotypes. Besides the finding that mutations in R1 and R2 motifs have differential effects in oogenesis, presumably because they mediate different protein interactions, the description of the *ari-1*^{2} phenotype seems uninformative toward the understanding of the normal function and it was not pursued further.

Taken together, the data from germline mosaics and fertility of viable transheterozygotes suggest that ARI-1 is not essential in oogenesis. The mutated version of ARI-1, in which the R1 motif is altered but R2 is still intact, is likely to mediate an aberrant interaction that can be ameliorated by progressive dilution with the normal product. This aberrant interaction seems to be most damaging in early embryogenesis, since transheterozygotes *ari-1*^{2}/*ari-1*^{1} survive relatively well to adulthood, provided that enough maternal deposit of the normal product was received during oogenesis. The observation that a mutated version of a protein is more deleterious than its absence is fairly common among proteins that become part of multimeric aggregates. In fact, the observed gene dosage effects suggest that ARI-1 might form multimeres and a yeast two-hybrid assay further supports this possibility (see below).

***ari-1* and *ari-2* are two nonredundant functions:** Concerning the function of the second family member, ARI-2, and its developmental implications, we refer to the information on the BDGP database (FlyBase). A single *P*-element insertion is available as the lethal mutant *l(2)07768*. This insert maps within the 5′ UTR sequence of *ari-2* mRNA. The reported embryonic and larval expression pattern of this insertion is ubiquitous, albeit particularly high in the central nervous system. We measured the lethal phase of this insertion and found it to be at earlier stages than that of *ari-1* mutants, in the first and second larval instars. On the other hand, double heterozygotes *ari-1*/+;*ari-2*/+ do not show visible phenotypes and the viability and fertility of this genotype is normal. Also, the lethal condition of either mutation cannot be rescued by two additional normal copies of the opposite *ari* gene. These observations indicate that the two genes are functionally distinct.

ARI proteins interact with an Ubc (ubiquitin-conjugating enzyme) through the first, but not the second, RING finger: In a coincident study, mouse ARI-1 and ARI-2 cDNA fragments have been isolated in a yeast two-hybrid screening using UbcM4 as a bait (Martinez-Noel *et al.* 1999). Also, in other independent studies, the complete human ARI-1 coding sequence has been reported by

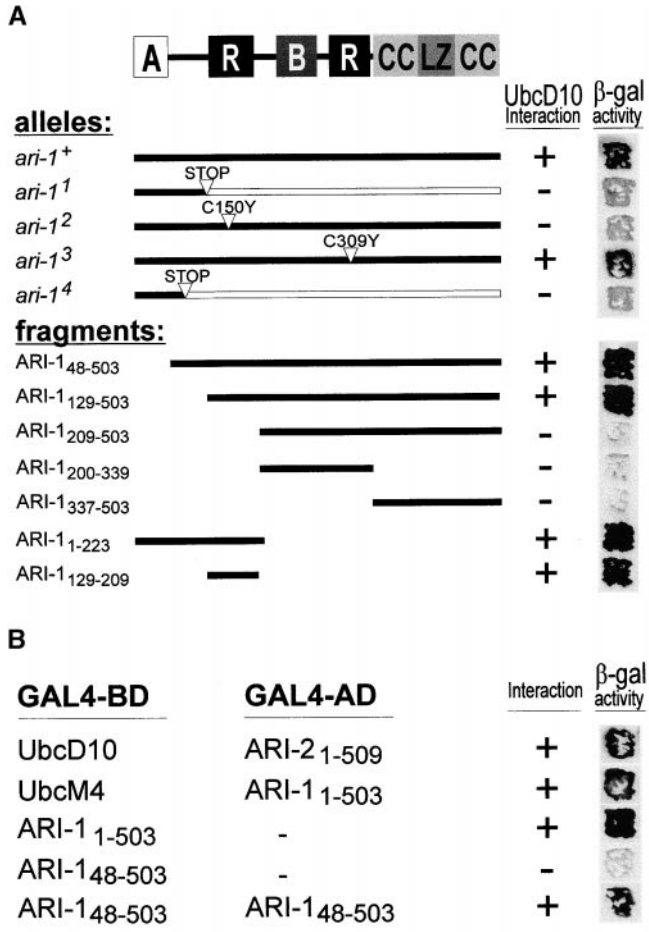

Figure 7.—Yeast two-hybrid interactions between UbcD10 and ARI proteins. (A) Structural dissection of ARI-1/UbcD10 interaction. Mutant alleles and fragments of ARI-1 (black bars) were expressed as GAL4 transactivation domain chimeras and tested for their ability to interact with complete UbcD10 fused to GAL4 DNA-binding domain. (B) Additional two-hybrid interactions. Subindexes indicate the stretch of amino acids in each fragment. The interaction was detected by β-galactosidase reporter activity in X-gal filter assays (photograph on the right).

two different groups as a UbcH7 interacting protein (see appendix). Mouse UbcM4 and human UbcH7 amino acid sequences are 100% identical.

These observations prompted us to search for the corresponding Drosophila counterpart of UbcM4 and to perform equivalent interaction tests. The Drosophila EST database includes a putative Ubc protein with 74% identity to UbcM4. The corresponding cDNA clones, obtained from BDGP, were sequenced and the gene was named *ubcD10* following the nomenclature for Ubc encoding genes in Drosophila (E.C. number: 6.3.2.19). The UbcD10 protein sequence contains the consensus pattern for the ubiquitin-conjugating enzyme's active site (PROSITE: PS00183). A UbcD10 fusion protein including the complete sequence was made with the yeast GAL4 DNA-binding domain (GAL4BD). The GAL4 transcriptional activation domain (GAL4AD) was fused

to wild-type and mutant versions of ARI-1, and direct protein-protein interaction with UbcD10 was assayed in the yeast two-hybrid system (Figure 7A). The results show an ARI-1/UbcD10 interaction that is abolished when N-terminal truncated versions of the protein are attempted (using mutant cDNA constructs from *ari-1*[1] and *ari-1*[4]). The same test was carried out with *ari-1*[2] and *ari-1*[3] versions, two mutations in key cysteines of R1 and R2 motifs, respectively (see above), and a differential effect was observed. The interaction with UbcD10 is prevented in the case of *ari-1*[2] but not *ari-1*[3], indicating that R1, but not R2, is required. To further substantiate this result, different fragments of ARI-1 were fused to GAL4AD and tested against the UbcD10-GAL4BD fusion protein (Figure 7). The data show that R1 is necessary and sufficient to mediate the interaction. Only chimeric proteins containing R1 retain the ability to interact with UbcD10. Furthermore, a small fragment containing R1 only [amino acid (aa)129–aa209] sustains the interaction. Control experiments were done by transformation and β-gal assays of all individual constructs and in coexpression with the complementary GAL4 separate domains. In the case of the complete ARI-1 sequence, an autonomous transcription activity was detected that must be due to the acid-rich N-terminal sequences since this activity was absent in the ARI-$1_{48–503}$ fragment. Also, ARI-1 and UbcD10-GAL4AD chimeras were tested for nonspecific interactions with human lamin C-GAL4BD with negative results.

Finally, the interaction was assayed for ARI-2/UbcD10 and for ARI-1/UbcM4, giving positive results in both cases (Figure 7B). Thus, it appears that the Ubc interaction might be a general feature of ARI proteins and that this interaction is conserved in mammals. An additional assay was carried out to test the possibility of ARI-1 dimerization. To this end, an ARI-1_{48-503} (lacking the acidic N-terminal region) fusion protein was made with GAL4BD, and the test gave a positive result (Figure 7B). This observation gives further support to the possibility that ARI-1 could form dimers.

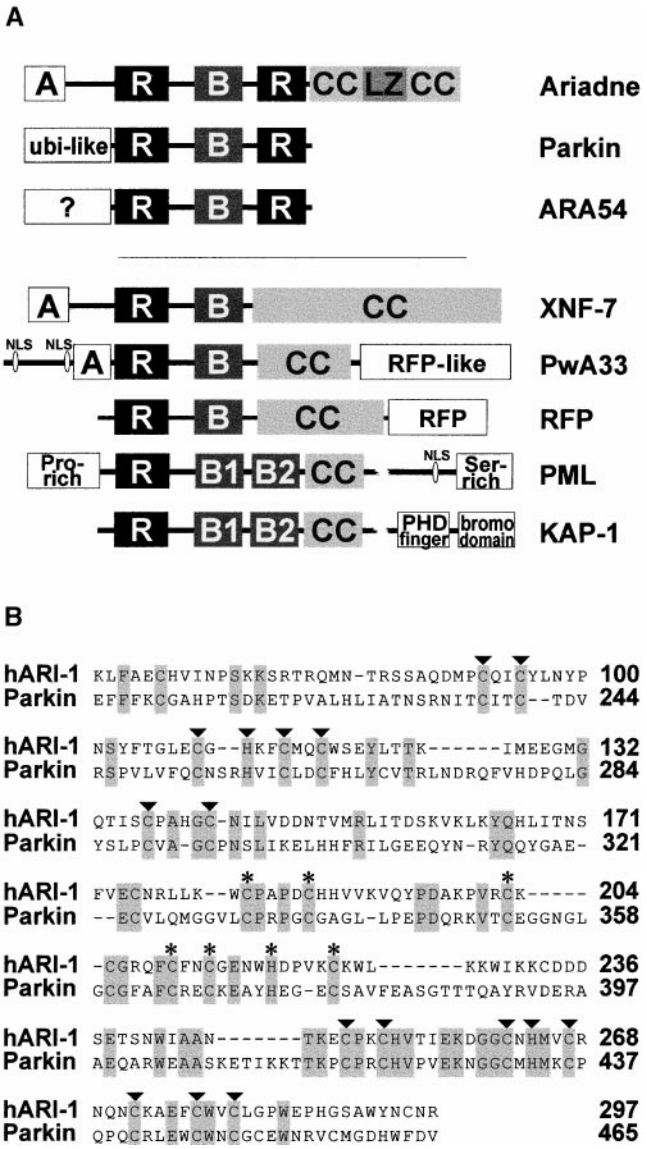

Figure 8.—ARI structural relatives. (A) Box diagrams of functionally characterized proteins showing the RBR (Parkin and ARA54) or the RBCC signatures. (B) Sequence comparison between the RBR domains of human ARI-1 and Parkin. Key amino acids are conserved in both proteins (shaded). The average identity in this region is 27%.

DISCUSSION

We report on ARIADNE-1, the first member of a conserved new family of proteins whose multiple structural domains include a RING finger that interacts with an E2 enzyme of the ubiquitin system. In Drosophila, *ari-1* is expressed in all tissues throughout development although the mutant phenotypes indicate differential requirements in tissues and developmental stages.

A new protein family: The primary sequence of ARI-1 serves to define a novel protein family characterized by the string of motifs ARBRCC. Drosophila ARI-1 and ARI-2 are the first two members of this family and conserved homologs in yeast, worms, mice, and humans have been identified as well. On the basis of structural criteria, ARI proteins are related to the RBCC family that is composed mostly by signal transducers and transcription factors (Figure 8A). In these proteins, the RBCC signature appears in conjuction with other motifs like bromodomain, RFP, and PHD fingers (Saurin *et al.* 1996). Within the string of motifs that the ARI family defines, we propose RBR as a new signature. As in the case of RBCC proteins, RBR is also found associated to other domains, *i.e.*, an ubiquitin-like domain in Parkin (see below) or an ill-defined N-terminal domain in ARA54 (Kang *et al.* 1999; Figure 8A). In addition, the RBR signature is found in many other functionally uncharacterized proteins across eukaryotic species. Most of these sequences are derived from genome projects

and their number is increasing rapidly, suggesting that RBR is an ancient and widespread modular element of protein structure (see appendix).

Functional role: ARI-1 becomes an additional case lending credence to the role that the ubiquitin system seems to play in neural connectivity. The first precedent was illustrated by the *bendless* mutant. This gene encodes a ubiquitin-conjugating enzyme whose depletion leads to neural defects (Muralidhar and Thomas 1993; Oh *et al.* 1994). The UbcD10 we have identified as interacting with ARI belongs to the same subfamily as UbcD3 encoded in *ben*. Mutations in *ben* have the most extreme effects in neural connectivity, particularly in the optic ganglia. Defective medulla rotation, the abnormal course of axon bundles, and reduced rhabdomeres, mostly R7, are reported as consistent features of *ben* eyes along with the original phenotype of incomplete bending of the cervical giant fiber axon. Adult muscles are also affected, albeit the tubular TDT to a greater extent than the indirect flight muscles (Edgecomb *et al.* 1993). Finally, *ben* null mutants are pupal lethals with a few short-lived and motor-impaired adult escapers. Mutant *ari-1* traits reported here coincide with those of *ben*; however, *ari-1* phenotypes are more extreme in every tissue analyzed. We have performed preliminary tests (double heterozygotes and gene dosage) searching for genetic evidence of interactions between *ari-1* and the nine Ubc encoding genes including *ben*, but no positive indication has been found so far. Thus, it seems that UbcD3 on the one hand and UbcD10 and ARI-1 on the other are components of two mechanisms within the ubiquitin system.

Considering the general expression of *ari-1*, it is likely that all cell types require its activity. However, at the light microscope level and under the procedures used, the mutant phenotypes become most evident in adult tissues. The failure to detect larval phenotypes cannot be justified, at least solely, on the basis of a large maternal deposit of the normal product. The germline mosaics of null mutations yield regular escapers identical in frequency and phenotype to those produced from heterozygous ovaries. It is more probable that the phenotypes in the larval tissues are subtler than in the adult, requiring a level of observation beyond that used here. It is worth noting that the cell types in which the mutant phenotypes are most apparent are those that require a massive and rapid membrane deposition, namely, macrobristles, photoreceptors, large tubular muscles, and rewiring neurons at metamorphosis. These processes represent a high demand on the physiology of the cell. In particular, proteins and membranous cisternae must be supplied efficiently.

We have detected a substantial reduction of rough endoplasmic reticulum (Figure 6) in mutant photoreceptors. This trait is more difficult to evaluate in other cell types because their ultrastructure is not as well characterized as that of the photoreceptors. However, this membrane system plays such a central role in the biology of the cell that it is plausible that it could account for the variety of phenotypes observed. The endoplasmic reticulum is the port of entry of most compartmentalized, membrane-anchored, and secretory proteins. It is also the site of folding and modification of nascent protein chains and assembly of multisubunit complexes. The ubiquitin pathway plays a central role in the "quality control" machinery to remove those proteins that fail to fold properly or to oligomerize, as has been demonstrated for the cystic fibrosis transmembrane conductance regulator and the T-cell receptor (Hershko and Ciechanover 1998). Interestingly, a RING-finger protein, Der3p / Hrd1p, is an integral component of a retrograde transport system in yeast endoplasmic reticulum (Bordallo *et al.* 1998). The system interacts with the 26S proteasome and includes a Ubc enzyme, Ubc7p. Also, mutations in the Drosophila *ninaA* cyclophilin homologue, involved in the protein folding and secretory pathway of rhodopsin 1, lead to an accumulation of endoplasmic reticulum in photoreceptors (Colley *et al.* 1991). The reduction of endoplasmic reticulum in *ari-1* mutant photoreceptors could indicate a role of ARI proteins in ubiquitin-mediated mechanisms. In turn, a reduced endoplasmic reticulum is a likely origin for the small rhabdomeres and short bristles that all alleles show.

Regarding the cellular compartment in which ARI-1 performs its function, the protein appears to localize mainly in the cytoplasm according to Western blots of cytoplasm *vs.* nuclear enriched fractions. Nevertheless, a transient nuclear localization cannot be formally excluded since a putative nuclear localization signal (Boulikas 1994), KKWIKK, can be found between amino acids 268 and 273. On the other hand, the N-terminal acid cluster shows the requirements for transcription activation domains (Triezenberg 1995) and, in a yeast reporter assay, we find this domain to be necessary for the autonomous transcription activity of the ARI-1-GAL4BD fusion. Thus, considering the multiple domains present in ARI-1, it is plausible that the protein might perform distinct interactions in several cellular compartments.

Interaction mechanisms: Cysteines 150 and 309 are key residues for the activity of each RING finger of ARI-1 since alleles *ari-1*^{2} and *ari-1*^{3} are full lethals. In addition, the C150Y version of the protein fails to sustain one of the identified interactions of ARI-1, that with UbcD10. These *in vivo* and *in vitro* observations coincide with findings in the breast / ovarian cancer susceptibility gene product BRCA-1 (Brzovic *et al.* 1998) where the RING motif of this human protein also mediates an interaction with a ubiquitin enzyme, the ubiquitin hydrolase BAP1 (Jensen *et al.* 1998). The implication of a RING-finger protein in the ubiquitin pathway raises the possibility that ARI-1 might be a substrate for UbcD10-mediated ubiquitination and targeted for degradation. ARI-1

Western blots show a single 59-kD band throughout development without any smear or ladder-like signals that could result from ubiquitin-mediated degradation. Although ARI-1 ubiquitination cannot be excluded at this point, a more likely role for ARI proteins might be the modulation of Ubc activity upon other substrates. Recent studies have shown common structural features among ubiquitination complexes such as SCF (Skp1-Cdc53/CUL1-F-box), APC (anaphase promoting complex), or VCB (*Von Hippel-Landau*-ElonginC-ElonginB). Apart from proteins with E2 and E3 activities, SCF, APC, and VCB also contain adaptor proteins with a variety of protein-protein interaction modules and a conserved domain (F-box or SOCS-box) (Tyers and Willems 1999). None of these domains are present in ARI proteins; thus, ARI might represent a new class of adaptor proteins in ubiquitination complexes. In fact, the recent identification of Rbx1 as a common component of SCF and VCB complexes (Kamura *et al.* 1999) already has introduced the RING-finger motif as a keystone in the combinatorial control of ubiquitination. Rbx1 is a RING-finger protein that interacts with E2 and E3 enzymes as well as with some adaptor proteins. These interactions are necessary to stimulate the catalytic activity of the fully assembled complex, thereby limiting its substrate specificity (Skowyra *et al.* 1999). This speculative proposal of ARI-1 as an adaptor in a multimeric complex need not be restricted to a ubiquitin tagging system. For example, the SUMO-1 or Rub-1 tagging systems share components with the ubiquitination complexes. In this context, PML, a RBCC protein involved in acute promyelocytic leukemia, is covalently modified by SUMO-1. This modification requires the interaction between Ubc9, a nuclear E2 enzyme, and the R motif in PML (Duprez *et al.* 1999).

Relevance to human pathologies: The interaction between ARI-1 and UbcD10 detected in the yeast two-hybrid assay is a conserved mechanism since mouse and fly homologues substitute for each other. Although a genetic test that could validate this interaction *in vivo* cannot be carried out at this point, the interspecific functional substitution is a strong argument to support its biological relevance. This functional substitution has a potential clinical interest. The sequence of human UbcH7 is 100% identical to UbcM4. In turn, UbcH7 is known to interact with E6-AP, a ubiquitin ligase that uses the tumor suppressor p53 as a substrate (Nuber *et al.* 1996). In addition, a defective E6-AP is implicated in Angelman's syndrome (Jiang *et al.* 1998). As a logical derivative from our data in Drosophila, the possible interaction between human ARI-1 and the doublet UbcH7/E6-AP should be considered.

Several human pathologies are caused by functional deficits in RING-finger proteins. Aside from PML and SIAH-1 discussed above, mutations that delete the RING motif of PEX10 cause defects in peroxisome biogenesis leading to Zellweger's syndrome (Okumoto *et al.* 1998). However, the most direct link with ARI proteins is found in *parkin*, a gene associated with juvenile parkinsonism (Kitada *et al.* 1998). During the search for sequence homologies, the Parkin protein was identified because of a RING-finger motif. Upon closer inspection, however, an RBR signature was evident (Figure 8B). In addition, this motif seems to be directly linked to the pathology as the disease can be caused by a point mutation, T240R (Hattori *et al.* 1998), which corresponds to the R1 motif in ARI-1. Since this protein also exhibits a ubiquitin-like domain, it has been proposed that Parkin might cause alterations in the ubiquitin system or defects in its own functional maturation eventually leading to selective neurodegeneration. Although defective ubiquitination is a common feature of cellular inclusions such as the Lewy bodies, a hallmark of Parkinson disease (Alves-Rodrigues *et al.* 1998), the juvenile form of parkinsonism does not exhibit Lewy's bodies. Also, the early onset of the disease points toward a developmental etiology. As an alternative mechanism to ubiquitination, Parkin could be involved in protein tagging of the SUMO-1 or Rub-1 type. In any event, two important questions arise from the results reported here: (1) Are human ARI proteins involved in the biology of Parkin? and (2) Does Parkin interact with a Ubc enzyme?

We appreciate the comments from lab members as well as the contributions of Dr. B. Haemmerle with the electron microscopy, Dr. L. Torroja for preliminary silver staining preparations, and P. Ochoa for technical help with nuclear extracts. Also, we thank Profs. P. Sternberg, K. Zinn, and P. Bjorkman (Caltech) for critical comments to an earlier version of this manuscript. The work was supported by grants PM 96-006 from the DGICYT (Spanish Ministry of Culture) and 8.5/0043/1998 from the Community of Madrid.

LITERATURE CITED

Alves-Rodrigues, A., L. Gregori and M. E. Figueiredo-Pereira, 1998 Ubiquitin, cellular inclusions and their role in neurodegeneration. Trends Neurosci. **21:** 516–520.

Ashburner, M., 1989 *Drosophila: A Laboratory Manual*. Cold Spring Harbor Laboratory Press, Cold Spring Harbor, NY.

Baldwin, A. S., 1996 The NF-kappa B and I kappa B proteins: new discoveries and insights. Annu. Rev. Immunol. **14:** 649–683.

Barlow, P. N., B. Luisi, A. Milner, M. Elliott and R. Everett, 1994 Structure of the C3HC4 domain by 1H-nuclear magnetic resonance spectroscopy: a new structural class of zinc-finger. J. Mol. Biol. **237:** 201–211.

Baumann, A., I. Krah-Jentgens, R. Muller, F. Muller-Holtkamp, R. Seidel *et al.*, 1987 Molecular organization of the maternal effect region of the *Shaker* complex of Drosophila: characterization of an Ia channel transcript with homology to vertebrate sodium channel. EMBO J. **6:** 3419–3429.

Blest, A. D., 1975 A new method for the reduced silver impregnation of arthropod central nervous systems. Proc. R. Soc. Lond. B Biol. Sci. **193:** 191–197.

Bordallo, J., R. K. Plemper, A. Finger and D. H. Wolf, 1998 Der3p/Hrd1p is required for endoplasmic reticulum-associated degradation of misfolded lumenal and integral membrane proteins. Mol. Biol. Cell **9:** 209–222.

Borden, K. L., and P. S. Freemont, 1996 The RING finger domain: a recent example of a sequence-structure family. Curr. Opin. Struct. Biol. **6:** 395–401.

Borden, K. L., M. N. Boddy, J. Lally, N. J. O'Reilly, S. Martin *et al.*, 1995 The solution structure of the RING finger domain

from the acute promyelocytic leukaemia proto-oncoprotein PML. EMBO J. **14:** 1532–1541.

Boulikas, T., 1994 Putative nuclear localization signals (NLS) in protein transcription factors. J. Cell. Biochem. **55:** 32–58.

Brzovic, P. S., J. Meza, M. C. King and R. E. Klevit, 1998 The cancer-predisposing mutation C61G disrupts homodimer formation in the NH2-terminal BRCA1 RING finger domain. J. Biol. Chem. **273:** 7795–7799.

Canal, I., I. Fariñas, M. Gho and A. Ferrús, 1994 The presynaptic cell determines the number of synapses in the Drosophila optic ganglia. Eur. J. Neurosci. **6:** 1423–1431.

Carthew, R. W., and G. M. Rubin, 1990 seven in absentia, a gene required for specification of R7 cell fate in the Drosophila eye. Cell **63:** 561–577.

Cenci, G., R. B. Rawson, G. Belloni, D. H. Castrillon, M. Tudor *et al.*, 1997 UbcD1, a Drosophila ubiquitin-conjugating enzyme required for proper telomere behavior. Genes Dev. **11:** 863–875.

Colley, N. J., E. K. Baker, M. A. Stamnes and C. S. Zuker, 1991 The cyclophilin homolog ninaA is required in the secretory pathway. Cell **67:** 255–263.

Coombe, P. E., and M. Heisenberg, 1986 The structural brain mutant Vacuolar medulla of Drosophila melanogaster with specific behavioral defects and cell degeneration in the adult. J. Neurogenet. **3:** 135–158.

Desterro, J. M., J. Thomson and R. T. Hay, 1997 Ubch9 conjugates SUMO but not ubiquitin. FEBS Lett. **417:** 297–300.

Drummond, D. R., E. S. Hennessey and J. C. Sparrow, 1991 Characterisation of missense mutations in the Act88F gene of Drosophila melanogaster. Mol. Gen. Genet. **226:** 70–80.

Duprez, E., A. J. Saurin, J. M. Desterro, V. Lallemand-Breitenback, K. Howe *et al.*, 1999 SUMO-1 modification of the acute promyelocytic leukaemia protein PML: implications for nuclear localisation. J. Cell Sci. **112:** 381–393.

Edgecomb, R. S., C. Ghetti and A. M. Schneiderman, 1993 Bendless alters thoracic musculature in Drosophila. J. Neurogenet. **8:** 201–219.

Everett, R. D., W. C. Earnshaw, J. Findlay and P. Lomonte, 1999 Specific destruction of kinetochore protein CENP-C and disruption of cell division by herpes simplex virus immediate-early protein Vmw110. EMBO J. **18:** 1526–1538.

Ferrús, A., S. Llamazares, J. L. de la Pompa, M. A. Tanouye and O. Pongs, 1990 Genetic analysis of the Shaker gene complex of Drosophila melanogaster. Genetics **125:** 383–398.

Freemont, P. S., 1993 The RING finger: a novel protein sequence motif related to the zinc finger. Ann. NY Acad. Sci. **684:** 174–192.

Fujita, S. C., S. L. Zipursky, S. Benzer, A. Ferrús and S. L. Shotwell, 1982 Monoclonal antibodies against the Drosophila nervous system. Proc. Natl. Acad. Sci. USA **79:** 7929–7933.

Harbers, K., U. Miller, A. Grams, E. Li, R. Jaenisch *et al.*, 1996 Provirus integration into a gene encoding a ubiquitin-conjugating enzyme results in a placental defect and embryonic lethality. Proc. Natl. Acad. Sci. USA **93:** 12412–12417.

Hattori, N., H. Matsumine, S. Asakawa, T. Kitada, H. Yoshino *et al.*, 1998 Point mutations (Thr240Arg and Ala311Stop) in the Parkin gene. Biochem. Biophys. Res. Commun. **249:** 754–758.

Hershko, A., 1997 Roles of ubiquitin-mediated proteolysis in cell cycle control. Curr. Opin. Cell Biol. **9:** 788–799.

Hershko, A., and A. Ciechanover, 1998 The ubiquitin system. Annu. Rev. Biochem. **67:** 425–479.

Hodges, M., C. Tissot and P. S. Freemont, 1998 Protein regulation: tag wrestling with relatives of ubiquitin. Curr. Biol. **8:** R749–R752.

Hu, G., and E. R. Fearon, 1999 Siah-1 N-terminal RING domain is required for proteolysis function and C-terminal sequences regulate oligomerization and binding to target proteins. Mol. Cell. Biol. **19:** 724–732.

Ishikawa, K., T. Nagase, M. Suyama, N. Miyajima, A. Tanaka *et al.*, 1998 Prediction of the coding sequences of unidentified human genes. X. The complete sequences of 100 new cDNA clones from brain which can code for large proteins in vitro. DNA Res. **5:** 169–176.

Jensen, D. E., M. Proctor, S. T. Marquis, H. P. Gardner, S. I. Ha *et al.*, 1998 BAP1: a novel ubiquitin hydrolase which binds to the BRCA1 RING finger and enhances BRCA1-mediated cell growth suppression. Oncogene **16:** 1097–1112.

Jiang, Y. H., D. Armstrong, U. Albrecht, C. M. Atkins, J. L. Noebels *et al.*, 1998 Mutation of the Angelman ubiquitin ligase in mice causes increased cytoplasmic p53 and deficits of contextual learning and long-term potentiation. Neuron **21:** 799–811.

Kamura, T., D. M. Koepp, M. N. Conrad, D. Skowyra, R. J. Moreland *et al.*, 1999 Rbx1, a component of the VHL tumor suppressor complex and SCF ubiquitin ligase. Science **284:** 657–661.

Kang, H. Y., S. Yeh, N. Fujimoto and C. Chang, 1999 Cloning and characterization of human prostate coactivator ARA54, a novel protein that associates with the androgen receptor. J. Biol. Chem. **274:** 8570–8576.

Kitada, T., S. Asakawa, N. Hattori, H. Matsumine, Y. Yamamura *et al.*, 1998 Mutations in the parkin gene cause autosomal recessive juvenile parkinsonism. Nature **392:** 605–608.

Klug, A., and J. W. Schwabe, 1995 Protein motifs 5. Zinc fingers. FASEB J. **9:** 597–604.

Koegl, M., T. Hoppe, S. Schenkler, H. D. Ulrich, T. U. Mayer *et al.*, 1999 A novel ubiquitination factor, E4, is involved in multiubiquitin chain assembly. Cell **96:** 635–644.

Landschulz, W. H., P. F. Johnson and S. L. McKnight, 1988 The leucine zipper: a hypothetical structure common to a new class of DNA binding proteins. Science **240:** 1759–1764.

Liakopoulos, D., G. Doenges, K. Matuschewski and S. Jentsch, 1998 A novel protein modification pathway related to the ubiquitin system. EMBO J. **17:** 2208–2214.

Lovering, R., I. M. Hanson, K. L. Borden, S. Martin, N. J. O'Reilly *et al.*, 1993 Identification and preliminary characterization of a protein motif related to the zinc finger. Proc. Natl. Acad. Sci. USA **90:** 2112–2116.

Lupas, A., M. Van Dyke and J. Stock, 1991 Predicting coiled coils from protein sequences. Science **252:** 1162–1164.

Martinez-Noel, G., R. Niedenthal, T. Tamura and K. Harbers, 1999 A family of structurally related RING finger proteins interacts specifically with the ubiquitin-conjugating enzyme UbcM4. FEBS Lett. **454:** 257–261.

Matuschewski, K., H. P. Hauser, M. Treier and S. Jentsch, 1996 Identification of a novel family of ubiquitin-conjugating enzymes with distinct amino-terminal extensions. J. Biol. Chem. **271:** 2789–2794.

Muralidhar, M. G., and J. B. Thomas, 1993 The Drosophila bendless gene encodes a neural protein related to ubiquitin-conjugating enzymes. Neuron **11:** 253–266.

Nagase, T., N. Seki, K. Ishikawa, A. Tanaka and N. Nomura, 1996 Prediction of the coding sequences of unidentified human genes. V. The coding sequences of 40 new genes (KIAA0161-KIAA0200) deduced by analysis of cDNA clones from human cell line KG-1. DNA Res. **3:** 17–24.

Nuber, U., S. Schwarz, P. Kaiser, R. Schneider and M. Scheffner, 1996 Cloning of human ubiquitin-conjugating enzymes UbcH6 and UbcH7 (E2-F1) and characterization of their interaction with E6-AP and RSP5. J. Biol. Chem. **271:** 2795–2800.

Oh, C. E., R. McMahon, S. Benzer and M. A. Tanouye, 1994 bendless, a Drosophila gene affecting neuronal connectivity, encodes a ubiquitin-conjugating enzyme homolog. J. Neurosci. **14:** 3166–3179.

Okumoto, K., R. Itoh, N. Shimozawa, Y. Suzuki, S. Tamura *et al.*, 1998 Mutations in PEX10 is the cause of Zellweger peroxisome deficiency syndrome of complementation group B. Hum. Mol. Genet. **7:** 1399–1405.

Prado, A., I. Canal, J. A. Barbas, J. Molloy and A. Ferrús, 1995 Functional recovery of troponin I in a Drosophila heldup mutant after a second site mutation. Mol. Biol. Cell **6:** 1433–1441.

Prado, A., I. Canal and A. Ferrús, 1999 The haplolethal region at the 16F gene cluster of Drosophila melanogaster: structure and function. Genetics **151:** 163–175.

Preston, C. M., M. C. Frame and M. E. Campbell, 1988 A complex formed between cell components and an HSV structural polypeptide binds to a viral immediate early gene regulatory DNA sequence. Cell **52:** 425–434.

Price, B. D., Z. Chang, R. Smith, S. Bockheim and A. Laughon, 1993 The Drosophila neuralized gene encodes a C3HC4 zinc finger. EMBO J. **12:** 2411–2418.

Reddy, B. A., and L. D. Etkin, 1991 A unique bipartite cysteine-histidine motif defines a subfamily of potential zinc-finger proteins. Nucleic Acids Res. **19:** 6330.

Reddy, B. A., L. D. Etkin and P. S. Freemont, 1992 A novel zinc

finger coiled-coil domain in a family of nuclear proteins. Trends Biochem. Sci. **17:** 344–345.

Régnier, C. H., C. Tomasetto, C. Moog-Lutz, M. P. Chenard, C. Wendling *et al.*, 1995 Presence of a new conserved domain in CART1, a novel member of the tumor necrosis factor receptor-associated protein family, which is expressed in breast carcinoma. J. Biol. Chem. **270:** 25715–25721.

Sambrook, J., E. F. Fritsch and T. Maniatis, 1989 *Molecular Cloning: A Laboratory Manual.* Cold Spring Harbor Laboratory Press, Cold Spring Harbor, NY.

Saurin, A. J., K. L. Borden, M. N. Boddy and P. S. Freemont, 1996 Does this have a familiar RING? Trends Biochem. Sci. **21:** 208–214.

Skowyra, D., D. M. Koepp, T. Kamura, M. N. Conrad, R. C. Conaway *et al.*, 1999 Reconstitution of G1 cyclin ubiquitination with complexes containing SCFGrr1 and Rbx1. Science **284:** 662–665.

Tranque, P., K. L. Crossin, C. Cirelli, G. M. Edelman and V. P. Mauro, 1996 Identification and characterization of a RING zinc finger gene (C-RZF) expressed in chicken embryo cells. Proc. Natl. Acad. Sci. USA **93:** 3105–3109.

Triezenberg, S. J., 1995 Structure and function of transcriptional activation domains. Curr. Opin. Genet. Dev. **5:** 190–196.

Tyers, M., and A. R. Willems, 1999 One ring to rule a superfamily of E3 ubiquitin ligases. Science **284:** 601, 603–601, 604.

Communicating editor: T. Schüpbach

APPENDIX

Gene	Organism	Genomic DNA	cDNA	Protein	Reference and notes
ari-1	*S. cerevisiae*	Z28242		P36113	
	C. elegans	AF003137			
	D. melanogaster	X98309	X98310	Q94981	
	M. musculus		AJ130977		
	H. sapiens		AJ130976		Partial sequence
	H. sapiens		AF072832		UbcH7-binding protein
	H. sapiens		AJ243190		UbcH7-binding protein
ari-2	*C. elegans*	U61944		Q22431	
	D. melanogaster	AC002473	AJ010169		
	M. musculus		AJ130975		
	H. sapiens		AJ130978		
Other RBR	*Arabidopsis thaliana*	AB005234			
	A. thaliana	AB018114			
	A. thaliana	AL035521			
	A. thaliana	AL004512			
	C. elegans	AF003137			
	C. elegans	U80847		P91067	
	C. elegans	U13644		Q20871	
	C. elegans	U13644		Q20874	
	H. sapiens	D79983			Nagase *et al.* (1996)
	H. sapiens	AB014608			Ishikawa *et al.* (1998)
	H. sapiens		165055		
ubcM4	*M. musculus*		X97042		Harbers *et al.* (1996)
ubcH7	*H. sapiens*		X92963		Nuber *et al.* (1996)
ubcD10	*Drosophia melanogaster*		AJ238007		
parkin	*H. sapiens*	AB009973		O60260	Kitada *et al.* (1998)
ara54	*H. sapiens*	AF060544			Kang *et al.* (1999)

Accession numbers correspond to GenBank and SPTREMBL databases for DNA and protein sequences, respectively.